Memoirs of the School of Engineering, Nagoya University
Vol.45. No.1 (1993)

ON THE NUMERICAL OUTFLOW BOUNDARY CONDITION OF THE VISCOUS FLOW AROUND A SQUARE CYLINDER

Ikuo NAKAMURA*, Takashi WATANABE** and Takashi YOSHIDA*

*Department of Mechano-Informatic Systems Engineering

**College of General Education

(Received May 31, 1993)

Abstract

The issue of open, or outflow, boundary conditions is important to the numerical simulation of incompressible viscous flows. But there are few studies of this problem because it is very difficult to give exact mathematical conditions for finite and artificial boundaries.

In this paper, four types of open boundary conditions are compared numerically in a two-dimensional flow past a square cylinder using a finite difference method. They are a free outflow condition and three kinds of Sommerfeld radiation conditions based on the free stream velocity at infinity, the Halpern's analysis, and the local velocity. The free outflow condition deforms velocity and pressure fields, while the Sommerfeld radiation condition using the free stream velocity has the least influence on the flow.

1. Introduction

Many problems in fluids mechanics are defined on unbounded domain. Numerical treatment of the boundary conditions (BCs) is an important issue. Kawaguti[1], in the earliest numerical simulation of a steady flow around a circular cylinder, projected the unbounded domain onto the bounded one and used an asymptotic solution at infinity as an boundary condition. However, it is impossible to extend this method to unsteady and high Reynolds number flows or flows around a complex geometry of which asymptotic solutions are generally unknown. Therefore we usually bound the domain and give artificial boundary conditions. Unfortunately, these BCs are not set by Nature, so no one can provide mathematically permissible BCs for Navier-Stokes equations[2]. Because these equations are elliptic, so that the exact solution is not determined without considering whole domain.

Many papers in the finite difference literature use the free outflow boundary condition, also called the zero gradient condition, for open or outflow boundary condition (OBC). These papers mainly discuss the results in upstream and local region, and little attention is devoted to the influence of BCs. Then we showed numerically in our previous paper[3] that it is inappropriate to apply the free outflow boundary condition to a wake of two-dimensional square cylinder.

On the other hand, Gresho and Sani[4] held the OBC Minisymposium (1991) to compare some OBCs and to find one that works best. The Sommerfeld radiation condition seemed to be good, which condition was first suggested by Sommerfeld[5] for a wave equation. Later, some form of this condition for Navier-Stokes equations were suggested. In this work, we will apply a free outflow BC and three kinds of Sommerfeld radiation condition to a two-dimensional flow around a square cylinder and compare them numerically.

2. Problem definition and boundary conditions

The two-dimensional flow around a square in an unbounded incompressible fluid will be considered. Mathematically, the boundary conditions at infinity are,

$$u=1,\ v=0,\ P=0 \qquad (\sqrt{x^2+y^2}\to\infty) \tag{1}$$

Here u and v are velocity components in the x- and y-directions, respectively, in a Cartesian reference frame; P is pressure. They are nondimensional form based on free stream velocity U_0, the length of the square side dimension H and the constant density ρ. In numerical simulations, we introduce the bounded computational domain as shown in Fig. 1 and give the artificial boundary conditions. At the inflow and side boundaries, the free stream conditions are applied. At the outflow boundary, the four types OBCs will be tested for the velocity.

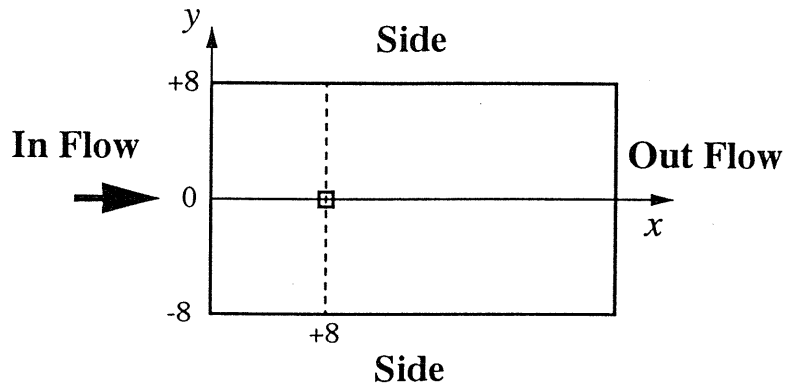

Fig. 1 Problem definition and coordinate.

OBC 1: free outflow condition[6]

$$\frac{\partial u}{\partial x}=\frac{\partial v}{\partial x}=0 \tag{2}$$

OBC 2: Sommerfeld radiation condition using the free stream velocity components; U=1 and V=0[7]

$$\frac{\partial u}{\partial t}+U\frac{\partial u}{\partial x}=0\ ,\quad \frac{\partial v}{\partial t}+U\frac{\partial v}{\partial x}=0 \tag{3}$$

OBC 3: Sommerfeld radiation condition by Halpern and Schatzman[8]

$$\frac{\partial u}{\partial t}+U\frac{\partial u}{\partial x}=0\ ,\quad \frac{\partial v}{\partial x}=0 \tag{4}$$

OBC 4: Sommerfeld radiation condition using the local velocity components; u and v[9]

$$\frac{\partial u}{\partial t}+u\frac{\partial u}{\partial x}+v\frac{\partial u}{\partial y}=0\ ,\quad \frac{\partial v}{\partial t}+u\frac{\partial v}{\partial x}+u\frac{\partial v}{\partial y}=0 \tag{5}$$

OBC 1 is based on the assumption that the computational domain is sufficiently long.

Radiation condition was introduced by Sommerfeld in order to solve the problem of oscillation which was defined on unbounded domain and had source of energy. He considered that energy radiating from the source should dissipate to infinity. Then at the boundary, the only wave equation radiating to out of domain was considered, and the equation for wave entering from infinity was vanished. For the flow problem, the radiation condition at the outflow boundary is

$$\frac{\partial u}{\partial t}+c\frac{\partial u}{\partial x}=0 \tag{6}$$

where c is a phase velocity of wave[10]. This condition requires that the flow is hyperbolic in nature. We consider as following for elliptic or parabolic systems.

The coordinate transformation from a frame fixed spatially to a frame moving with the free stream velocity, U=1 and V=0, lead to;

$$\begin{cases} x'=x-Ut \\ y'=y \\ t'=t \end{cases} \qquad \begin{cases} u'=u-U \\ v'=v \end{cases}$$

where prime denotes any variable associated with the moving frame. Then we assume that near the outflow boundary diffusion is small, and the flow is approximately steady in the moving frame;

$$\frac{\partial u'}{\partial t'} = 0 \tag{7}$$

The equation (7) becomes (3) in the fixed frame and that equation is the same one representing the Taylor's hypothesis[11], which is linear and hyperbolic. Then it's general solution is;

$$u(x, t) = f(x - Ut)$$

which is determined by the flow upstream in a zone of dependence.

OBC 3 is suggested by Halpern and Schatzman for the Oseen equations. We investigate whether this OBC is appropriate for a nonlinear flow.

Nataf was employed the nonlinear equations (5) replaced U and V in the linear equations (3) on local velocities, u and v for simulation of the steady flow past a two-dimensional ellips. We investigate whether this OBC is appropriate for a unsteady flow.

For the pressure OBC, we employ the Neumann BC obtained by applying the normal component of the momentum equation on outflow boundary[12].

3. Numerical Method

The governing equations are the Navier-Stokes equations and continuity equation for a unsteady incompressible viscous flow;

$$\frac{\partial \mathbf{u}}{\partial t} + (\mathbf{u} \cdot \nabla)\mathbf{u} = -\nabla P + \frac{1}{Re}\nabla^2 \mathbf{u} \tag{8}$$

$$div\,\mathbf{u} = 0 \tag{9}$$

where Re is the Reynolds number. The pressure Poisson equation is derived by operating on (8) with divergence operator to give,

$$\nabla^2 P = -div\{(\mathbf{u} \cdot \nabla)\mathbf{u}\} + \frac{1}{Re}\nabla^2 D - \frac{\partial D}{\partial t} \tag{10}$$

where $D=div\mathbf{u}$. We solve (8) and (10) using the numerical procedures based on the MAC method[13]. First, we calculate P^{n+1} from (10) assuming D^{n+1} is zero,

$$\nabla^2 P^{n+1} = -div\{(\mathbf{u}^n \cdot \nabla)\mathbf{u}^n\} + \frac{D^n}{\Delta t} \tag{11}$$

where n is the integration time step. For the time integration of (8), the Euler backward scheme is used except the nonlinear convection terms which are linearized by evaluating the convection velocity at n level,

$$\frac{\mathbf{u}^{n+1} - \mathbf{u}^n}{\Delta t} + (\mathbf{u}^n \cdot \nabla)\mathbf{u}^{n+1} = -\nabla P^{n+1} + \frac{1}{Re}\nabla^2 \mathbf{u}^{n+1} \tag{12}$$

The third order upwind difference scheme by Kawamura and Kuwahara[14] is employed for the spatial discretization of the convection terms,

$$u\frac{\partial u}{\partial x}\Big)_i = u_i\frac{-u_{i+2}+8(u_{i+1}-u_{i-1})+u_{i-2}}{12\Delta x} + \frac{1}{4}|u_i|\frac{u_{i+2}-4u_{i+1}+6u_i-4u_{i-1}+u_{i-2}}{\Delta x} \tag{13}$$

The other terms are discretized by the second order central difference scheme. The Neumann type BCs are discretized by the second order upwind scheme. The resulting set of algebraic difference equations is solved iteratively using the incomplete LU decomposition conjugate gradient squared (ILUCGS) method.

The numerical grid is a uniform and non-staggered one with grid increment $\Delta x=\Delta y=0.1$, and the time increment is $\Delta t=0.01$. The Reynolds number is 100. All our calculations were performed on the FACOM VP2600 at Nagoya University Computation Center.

4. Numerical Results

4.1. Computational conditions

We tested seven cases as shown Table 1, to compare the influence of different OBCs. Computations are performed on two regions. One is a short region, $-8\leq y\leq+8$, $0\leq x\leq 28$, and the other is a long region, $-8\leq y\leq+8$, $0\leq x\leq 68$. All the instantaneous results are the values of various quantities at a particular time in the vortex shedding cycle. This time is chosen to be the instant when the lift coefficient C_L is changing from a negative value to a positive value; i.e. passing through zero from below.

Table 1. Computational conditions.

Case	OBC	Outflow Boundary	Grid
Case 1	OBC1	$x=28.0$	281×181
Case 2	OBC2	$x=28.0$	281×181
Case 3	OBC3	$x=28.0$	281×181
Case 4	OBC4	$x=28.0$	281×181
Case 5	OBC1	$x=68.0$	681×181
Case 6	OBC2	$x=68.0$	681×181
Case 7	OBC4	$x=68.0$	681×181

4.2. Results on the long region

Fig. 2(e), 2(f) and 2(g) are instantaneous pressure contours on the long region. Although these contours disagree near outflow boundary due to the influence of different OBCs, they agree qualitatively near the square. In many previous papers which compared deferent numerical methods or numerical conditions, mainly qualitative judgments were made and quantitative evaluations were not sufficient. We define the following integration value to evaluate

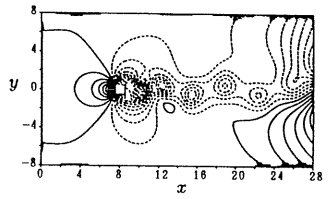

(a) Case 1

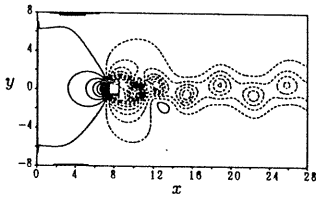

(b) Case 2

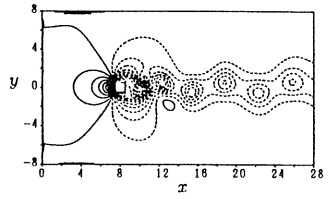

(c) Case 3

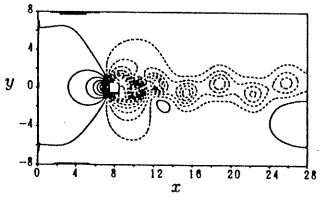

(d) Case 4

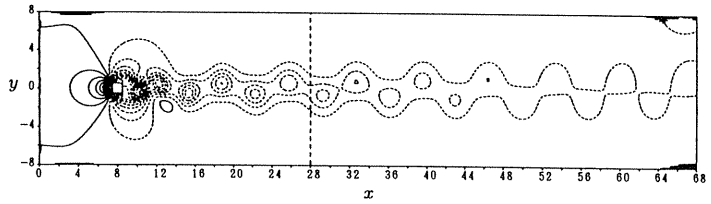

(e) Case 5

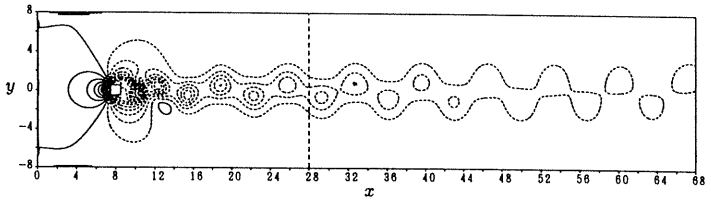

(f) Case 6

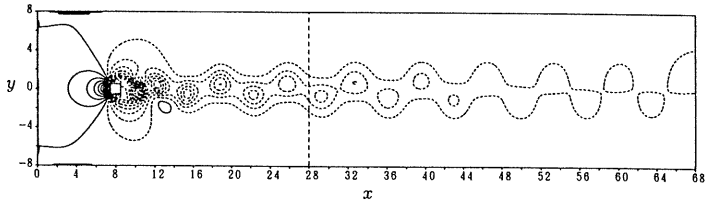

(g) Case 7

Fig. 2 Pressure contours.

quantitatively the difference between each cases;

$$\phi_e(x,t) = \left\{ \int_{y=-8}^{y=+8} (\phi(x,y,t) - \phi_{\text{Case 6}}(x,y,t))^2 dy \right\}^{\frac{1}{2}} \tag{14}$$

where ϕ is an arbitrary variable. Equation (14) is the integration of difference between the solution of Case 6 and the other case over y at any section of x. This is similar to usual L^2 norm of the functional analysis. The subscript e denotes the integration value of (14). Since $\phi_e(0,t)$ equal zero due to the same Dirichlet boundary condition at the inflow boundary, that value at x=0 is excepted in figures of ϕ_e which will be shown later.

Fig. 3 shows instantaneous u_e, v_e and P_e of Case 5 and Case 6. As x approches the outflow boundary, each value becomes large. For comparison, the integration values of the solution of Case 6 itself, defined as following, are also shown.

$$\phi_s(x,t) = \left\{ \int_{y=-8}^{y=+8} (\phi_{\text{Case 6}}(x,y,t))^2 dy \right\}^{\frac{1}{2}} \tag{15}$$

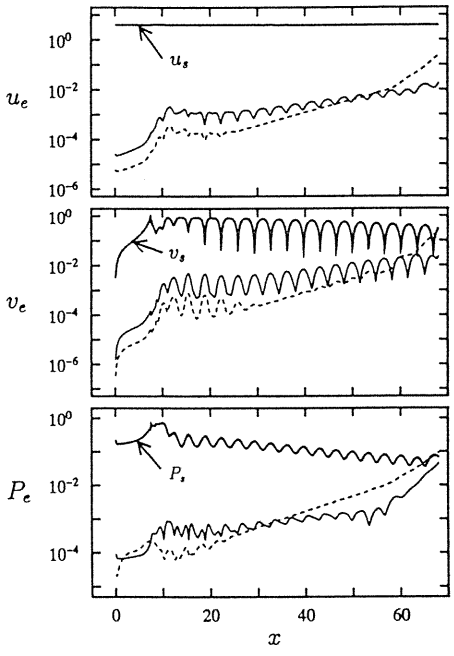

Fig. 3 Variation of the integration values u_e, v_e and P_e with x on the long region.
------ Case 5 ——— Case 7

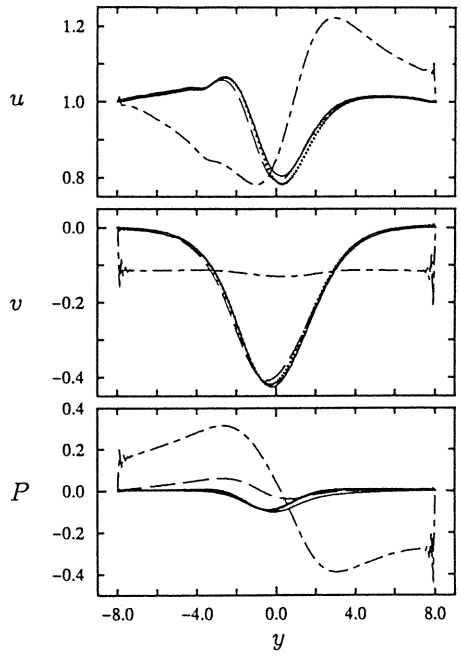

Fig. 4 Instantaneous velocity and pressure profiles at x=28.
——— Case 1 ------ Case 2
——— Case 3 ——— Case 4
· · · · · Case 6

In the upstream region from x=28, where the same position with the outflow boundary on the short region, u_e of Case 5 and 7 are less than 1% of u_s, and P_e of Case 5 and 7 are also less than 1% of P_s. v_s changes periodic in x direction. The position of minimum of v_s corresponds to the center of each vortex, where v_e becomes relatively large and about 10% of v_s. But v_e at other position is enough small for v_s. Therefore we regard the solution of Case 6 as 'exact' one when we discuss the results on the short region.

4.3. *Results on the short region*

Fig. 2(a), 2(b), 2(c) and 2(d) show instantaneous pressure contours of Cases 1 ~ 4 on the short region. In Case 1, large pressure gradient in y direction occurs at the outflow boundary. In Case 4, positive pressure region occurs near the outflow boundary. On the other hand, the

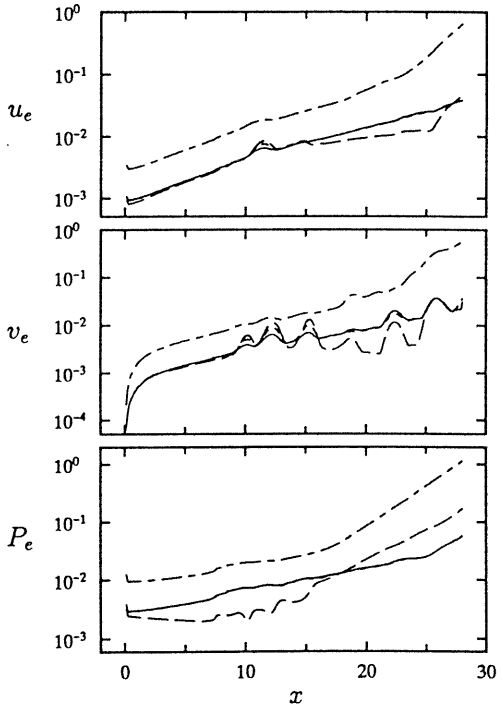

Fig. 5 Variation of integration values u_e, v_e and P_e with x on the short region.
——— Case 1 – – – – – – Case 2
——— Case 3 ——— Case 4

Table 2. Integration values u_e, v_e and P_e at x=28 on the short region.

Case	u_e	v_e	P_e
Case1	6.476×10^{-1}	5.497×10^{-1}	$1.136 \times 10^{+0}$
Case2	3.895×10^{-2}	2.322×10^{-2}	5.808×10^{-2}
Case3	3.842×10^{-2}	3.088×10^{-2}	5.662×10^{-2}
Case4	4.951×10^{-2}	3.645×10^{-2}	1.695×10^{-1}

contours of Case 2 and Case 3 are quite similar with those of Case 6. Fig. 4 shows the instantaneous velocity and pressure profiles at x=28. Those of Case 1 are clearly different form other cases. In Case 1, v is nearly constant and P has large gradient near x=0. Near the side boundary, u, v and P oscillate considerably and are not smooth solutions. By contrast, the profiles of Case 2, 3 and 4 seem to be similar qualitatively. Then, we show the variations of u_e, v_e and P_e with x in Fig. 5 and the values of them at x=28 in Table 2. All values of Case 1 are much larger than other cases. The values of Case 2 agree with those of Case 3, so that we can not distinguish them except at x=28, where especially v_e of Case 3 is slightly larger than the one of Case 2. Though the values of Case 4 are partially smaller than those of Case 2 and Case 3, they increase rapidly as close the outflow boundary, so that P_e of Case 4 at x=28 is especially larger than ones of Case 2 and 3.

It is important whether the given OBC is able to approximate well the natural outflow of vorticity at the boundary or not. Fig. 6 shows instantaneous vorticity contours. Fig. 6(e) is the result of Case 6, the 'exact' solution, and the periodic vortex pattern due to Kármán Vortex Street are observed in it. The distribution of vorticity obtained with Case 2 is much similar to Case 6. In Case 1 and Case 3 the sign of vorticity is inverted and negative value occur close the outflow boundary. In contrast, in Case 4 the region of positive vorticity is larger than

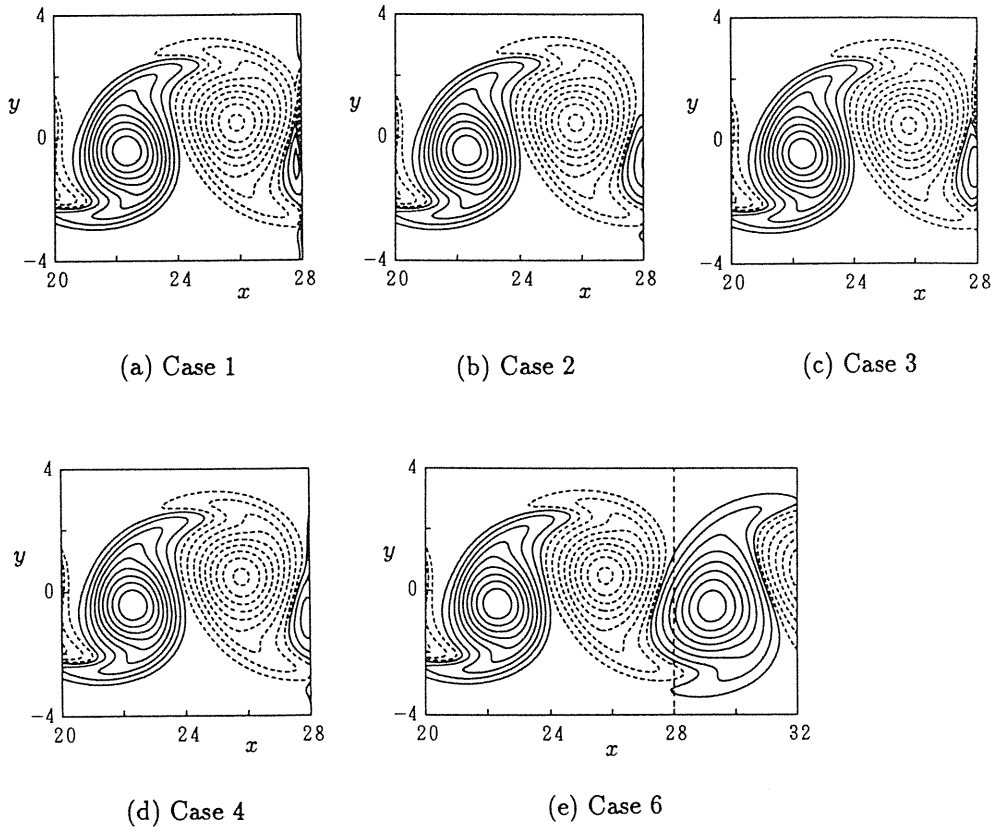

Fig. 6 Vorticity contours.

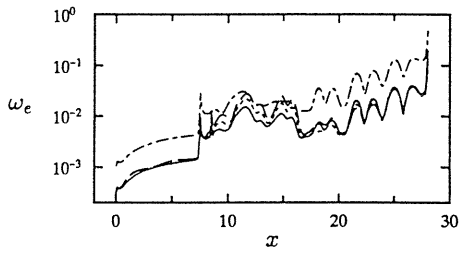

(a) whole region

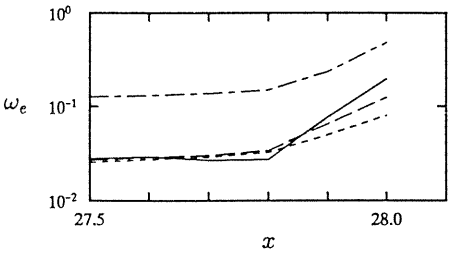

(b) near the outflow boundary

Fig. 7 Variation of integration values ω_e with x on the short mesh.
——— Case 1 ------ Case 2
——— Case 3 ——— Case 4

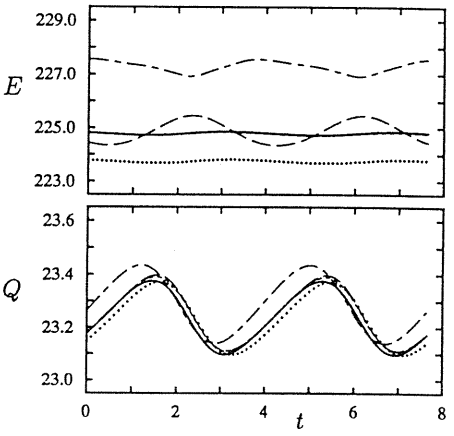

Fig. 8 Temporal variations of the kinetic energy norm E and the enstrophy Q.

Case 6. For the quantitative evaluation of the vorticity distribution, we define ω_e as the integration of difference of ω based on (14). The variation of ω_e with x are shown in Fig. 7(a) for the whole region and in Fig. 7(b) for the partially region near the outflow boundary. ω_e of all cases have the maximum value at the outflow boundary. The maximum value of Case 2 is smallest in the four cases on the short region.

4.4. Comparison of integration parameters and norms

Some integration parameters, a Strouhal number St, a lift coefficient C_L and a drag coefficient C_D, are very important for a flow around a structure. These parameters are given in Table 3 where notation denotes the time mean value. We suggested in previous paper that $\overline{C_D}$ tend to be influenced by OBC. $\overline{C_D}$ of Case 5, 6 and 7 on the long region, are the same and have little influence from each OBCs. However the period of shedding cycle T on the short region is shorter and $\overline{C_D}$ is larger than the results on the long region. Especially $\overline{C_D}$ of Case 1 is largest among four cases on the short region and it's difference from the result on the long region is also largest.

Table 3. Integration parameters.

Case	T	St	C_L	$\overline{C_D}$
Case1	7.64	0.1309	±0.448	1.633
Case2	7.66	0.1305	±0.450	1.627
Case3	7.67	0.1304	±0.450	1.627
Case4	7.66	0.1305	±0.451	1.627
Case5	7.68	0.1302	±0.451	1.624
Case6	7.67	0.1304	±0.450	1.624
Case7	7.68	0.1302	±0.450	1.624

We introduce two norms for quantitative evaluation of velocity fields on whole computational domain. They are the kinetic energy norm E and the enstrophy Q, as follows;

$$E = \int_{y=-8}^{y=+8} \int_{x=0}^{x=28} \frac{1}{2}\mathbf{u}^2 dxdy \tag{16}$$

$$Q = \int_{y=-8}^{y=+8} \int_{x=0}^{x=28} \frac{1}{2}\omega^2 dxdy \tag{17}$$

Fig. 8 shows the temporal variations of E and Q. The origin of time corresponds to the instant when the lift coefficient C_L of each case is changing from a negative value to a positive value. The temporal variations of E obtained Case 1 and Case 4 are obviously different form one of Case 6 for those mean value and phase. The value of Case 2 agree with one of Case 3. The phase and amplitude of both cases are similar with Case 6, though the mean value of both cases are larger than that of Case 6. The kinetic energy on each grid point are same order and contribute to integration of the kinetic energy norm identicaly except grid points close the wall boundary of a cylinder. Then the differences of the kinetic energy norm due to the difference of verocity fileds near the outflow boundary are obviously observed in Fig. 8. On the other hand, the difference of the enstrophy between each case is small. Since the magnitude of vorticity near the outflow boundary is quite smaller than that near the wall of a square cylinder, the difference of vorticity near the outflow boundary due to the influence of OBCs contribute little to the integration over the whole domain and does not give any obvious difference to the enstrophy.

5. Discussion

We summarize and discuss the results of the previous section. The free outflow boundary condition implicitly imposes $\partial v/\partial y=0$ in addition to (2), because $\partial v/\partial y=0$ is derived from the free boundary condition and the continuity equation (9). As the result, v of Case 1 is nearly constant at the outflow boundary, as shown in Fig. 4. It is physically incorrect that v is always constant with y in the wake, so that the results obtained with OBC 1 on the short region are quite different from the 'exact' results on the long region. This condition has been used commonly in the finite difference method, but there are some questions about it's appropriateness.

In contrast, the results of three types Sommerfeld radiation condition on the short region are similar with those on the long region. The values of u_e, v_e, P_e and ω_e in OBC 2 are smallest respectively at the outflow boundary. Also, the variation of the energy norm in OBC 2 agree with the result on the long region. Therefore this condition is most accurate in the four types OBCs tested here.

The results obtained with OBC 3, the Sommerfeld radiation condition by Halpern and Schatzman, agree with those of OBC 2 in upstream region. It is due to the same condition with OBC 2 for u. But v_e and ω_e are slightly larger than the results of OBC 2 at the outflow boundary and the vorticity of OBC 3 has a inverted sign as shown in Fig. 6(c). It is due to the different condition of v; i.e. $\partial v/\partial x=0$.

OBC 4, the Sommerfeld radiation condition using the local velocity, was applied for the steady flow by Nataf. However, Lugt and Haussling[15] pointed out that it is unacceptable to use the local velocity $\mathbf{u}$ which implies that ∇P is neglected. Because the vortices in the wake are of Hamel-Oseen type and thus have a pressure distribution with non-vanishing ∇P, which was experimentally shown by Timme[16]. The value of P_e obtained with OBC 4 is large near the outflow boundary, then OBC 4 seems not to be able to evaluate pressure accurately. Therefore OBC 4 is not appropriate for the unsteady vortex shedding flow. But for the steady flow, OBC 4 may be good as shown by Nataf, since the local velocity in the steady wake has little temporal variation and is nearly equal to the mean velocity.

The above discussion suggests that the Sommerfeld radiation condition using the free stream velocity is best among the four types OBCs tested in this study. The Navier-Stokes equations may have hyperbolic nature approximately in the wake and the Taylor's hypothesis works well.

6. Conclusions

The conclusions that can be drawn from this study are as follows.

1. The free outflow boundary condition is physically inappropriate and deform both velocity and pressure fields near the outflow boundary.
2. The results of the Sommerfeld radiation condition using the free stream velocity on the short region are most similar with the results on the long region among the four types OBCs tested in this study.
3. The results of the Sommerfeld radiation condition by Halpern and Schatzman agree with those of the condition using free stream velocity, except near the outflow boundary where the vorticity has a inverted sign.
4. The Sommerfeld radiation condition using the local velocity gives the larger error for pressure.

References

1) Kawaguti, M., Numerical solution of the Navier-Stokes equations for the flow around a circular cylinder at Reynolds number 40, J. Phys. Soc. Jap., Vol.8, No.6, p.747 (1953).
2) Gresho, P.M., Some interesting issues in incompressible fluid dynamics, both in the continuum and in numerical simulation, Adv. Appl. Mechanics, Vol.28, p.45 (1992), Academic Press.
3) Yoshida, T., Nakamura, I. and Watanabe, T., Effect of boundary conditions and finite difference schemes on the numerical analysis of a flow pase a square cylinder, Trans. JSME, Vol.59, p.374 (1993), in Japanease.

4) Gresho, P.M. and Sani, R.L., Announcement—Open boundary conditions (OBC) minisymposium, Int. J. Numer. Methods Fluids, Vol.11, p.949 (1990).
5) Sommerfeld, A.J.W., "*Vorlesungen über theoretische physik, VI. Partielle differentialgleichungen der physik*", Academie (1949), Leipzig.
6) Tamura, T. and Kuwahara, K., On the reliability of two-dimensional simulation for unsteady flows around a cylinder-type structure, J. Wind Engrg. Ind. Aerodyn., Vol.35, p.275 (1990).
7) Bottaro, A., Note on open boundary conditions for elliptic flows, Numer. Heat Transfer B, Vol.18, p.243 (1990).
8) Halpern, L. and Schatzman, M., Artificial boundary conditions for incompressible viscous flows, SIAM J. Math. Anal., Vol.20, No.2, p.308 (1989).
9) Nataf, F., An open boundary condition for the computation of the steady incompressible Navier-Stokes equations, J. Comput. Phys., Vol.85, p.104 (1989).
10) Orlanski, I., A simple boundary condition for unbounded hyperbolic flows, J. Comput. Phys., Vol.21, p.251 (1976).
11) Hinze, J.O., *"Turbulence"*, p.46 (1975), McGraw-Hill, NY.
12) Gresho, P.M. and Sani, R.L., On pressure boundary conditions for the incompressible Navier-Stokes equations, Int. J. Numer. Methods Fluids, Vol.7, p.1111 (1987).
13) Harlow, F.H. and Welch, J.E., Numerical calculation of time-dependent viscous incompressible flow of fluid with free surface, Phys. Fluids, Vol.8, No.12, p.2182 (1965).
14) Kawamura, T. and Kuwahara, K., Computation of high Reynolds number flow around a circular cylinder with surface roughness, AIAA Paper, 84-0340 (1984).
15) Lugt, H.J. and Haussling, H.J., Laminar flow past an abruptly accelerated elliptic cylinder at 45° incidence, J. Fluid Mech., Vol.65, p.711 (1974).
16) Timme, A., Über die Geschwindigkeitsverteilung in Wirbeln, Ing. Arch., Vol.25, p.205 (1957).